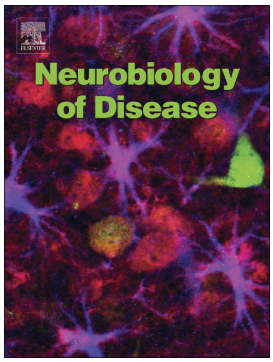

X-linked Dystonia-Parkinsonism patient cells exhibit altered signaling via nuclear factor-kappa B

Christine A. Vaine, David Shin, Christina Liu, William Hendriks, Jyotsna Dhakal, Kyle Shin, Nutan Sharma, Cristopher Bragg

PII: S0969-9961(16)30299-6
DOI: doi: 10.1016/j.nbd.2016.12.016
Reference: YNBDI 3883

To appear in: *Neurobiology of Disease*

Received date: 26 September 2016
Revised date: 17 November 2016
Accepted date: 18 December 2016

Please cite this article as: Christine A. Vaine, David Shin, Christina Liu, William Hendriks, Jyotsna Dhakal, Kyle Shin, Nutan Sharma, Cristopher Bragg , X-linked Dystonia-Parkinsonism patient cells exhibit altered signaling via nuclear factor-kappa B. The address for the corresponding author was captured as affiliation for all authors. Please check if appropriate. Ynbdi(2016), doi: 10.1016/j.nbd.2016.12.016

X-linked Dystonia-Parkinsonism patient cells exhibit altered signaling via nuclear factor-kappa B

Christine A. Vaine[a,b], David Shin[a,b], Christina Liu[a,b], William Hendriks[a,b], Jyotsna Dhakal[a,b], Kyle Shin[a,b], Nutan Sharma[a], D. Cristopher Bragg[a,b,*]

Affiliations

[a]The Collaborative Center for X-linked Dystonia Parkinsonism, Department of Neurology, Massachusetts General Hospital, Charlestown, MA 02129 USA

[b]Harvard Brain Science Initiative, Harvard Medical School, Boston, MA 02114 USA

*Corresponding Author:

D. Cristopher Bragg, Ph.D., Neuroscience Center and Department of Neurology, Massachusetts General Hospital-East, Building 149, 13th Street, Charlestown, MA 02129 USA. Phone: 617-643-5754, Fax: 617-724-1537, Email: bragg@helix.mgh.harvard.edu

Running title: Altered NFκB in XDP

Abstract

X-linked Dystonia-Parkinsonism (XDP) is a progressive neurodegenerative disease involving the loss of medium spiny neurons within the striatum. An XDP-specific haplotype has been identified, consisting of seven sequence variants which cluster around the human *TAF1* gene, but a direct relationship between any of these variants and disease pathogenesis has not yet been demonstrated. Because the pathogenic gene lesion remains unclear, it has been difficult to predict cellular pathways which are affected in XDP cells. To address that issue, we assayed expression of defined gene sets in XDP vs. control fibroblasts to identify networks of functionally-related transcripts which may be dysregulated in XDP patient cells. That analysis derived a 51-gene signature distinguishing XDP vs. control fibroblasts which mapped strongly to nuclear factor-kappa B (NFκB), a transcription factor pathway also implicated in the pathogenesis of other neurodegenerative diseases, including Parkinson's (PD) and Huntington's disease (HD). Constitutive and TNFα-evoked NFκB signaling was further evaluated in XDP vs. control fibroblasts based on luciferase reporter activity, DNA binding of NFκB subunits, and endogenous target gene transcription. Compared to control cells, XDP fibroblasts exhibited decreased basal NFκB activity and decreased levels of the active NFκB p50 subunit, but increased target gene expression in response to TNFα. NFκB signaling was further examined in neural stem cells differentiated from XDP and control induced pluripotent stem cell (iPSC) lines, revealing a similar pattern of increased TNFα responses in the patient lines compared to controls. These data indicate that an NFκB signaling phenotype is present in both patient fibroblasts and neural stem cells, suggesting this pathway as a site of dysfunction in XDP.

Abbreviations

ANOVA, analysis of variance; AR, androgen receptor; DMEM, Dulbecco's modified Eagle's medium; DSC; Disease-specific sequence change; ELISA, enzyme-linked immunosorbent assay; GLuc, *Gaussia* luciferase; HD, Huntington's disease; HRP, horseradish peroxidase; IFNγ, interferon gamma; IκB, inhibitor of kappaB proteins; IKK; IκB kinase complex; IPA®, Ingenuity® Pathway Analysis; iPSC, induced pluripotent stem cell; LDS, lithium dodecyl sulfate; LPS, lipopolysaccharide; LRRK2, leucine-rich repeat kinase-2; MOI, multiplicity of infection; MTS, multiple transcript system; NFκB, nuclear factor-kappa B; NSC, neural stem cell; O.D., optical density; PAGE, polyacrylamide gel electrophoresis; PBS, phosphate buffered saline; PD, Parkinson's disease; PINK1, PTEN-induced putative kinase-1; Pol II, RNA polymerase II; PVDF, polyvinylidene fluoride; RIPA, radioimmunoprecipitation assay buffer; RLU, relative light unit; ROCK, Rho-associated coiled-coil containing protein kinase; SDS, sodium dodecyl sulfate; SINE, short interspersed element; SVA, short interspersed nuclear element, variable number of tandem repeats, and Alu composite; TAF1, TATA binding protein-associated factor-1; TBS-T, Tris-buffered saline-Tween; TFIID, transcription factor IID complex; TLR, Toll-like receptor; TNFα, tumor necrosis factor alpha; TRAF, TNF receptor-associated factor; VNTR, variable number of tandem repeats; XDP, X-linked Dystonia-Parkinsonism

Keywords

XDP, NFκB, TAF1, fibroblasts, NSCs, DYT3

Introduction

X-Linked Dystonia-Parkinsonism (XDP) is a rare neurodegenerative disease characterized by adult-onset, progressive dystonia which over time is combined with or replaced by features of parkinsonism (Evidente et al., 2002a; Evidente et al., 2002b; Lee et al., 1991; Lee et al., 2002; Lee et al., 2011). The disease has been associated with the loss of medium spiny neurons within the striatum (Goto et al., 2013; Goto et al., 2005), although the involvement of other brain regions has not been definitively excluded, and the mechanisms underlying XDP neuropathology are not known. XDP primarily affects men from the island of Panay, Philippines, where the reported disease prevalence is approximately 5.74 cases per 100,000 individuals (Lee et al., 2011). It has been hypothesized that the disorder arises due to a founder mutation in this population, but identifying the pathogenic gene variant has proven difficult. Genetic studies over many years have culminated in the discovery of an XDP-specific haplotype consisting of seven sequence variants which affected individuals appear to inherit in a consistent "all or none" fashion (Domingo et al., 2015; Graeber and Muller, 1992; Haberhausen et al., 1995; Herzfeld et al., 2007; Kupke et al., 1992; Muller et al., 1994; Nemeth et al., 1999; Nolte et al., 2003; Wilhelmsen et al., 1991). These variants consist of five single nucleotide substitutions, designated Disease-specific Sequence Changes (DSC)-1,2,3,10,12, a 48-bp deletion, and a SINE-VNTR-Alu (SVA)-type retrotransposon insertion (Makino et al., 2007; Nolte et al., 2003). Because XDP patients reportedly bear all seven markers, none of which have ever been identified in ethnically-matched control subjects (Domingo et al., 2015), it has not yet been possible to pinpoint which, if any, of these variants may be pathogenic.

The seven haplotype markers cluster in and around the *TAF1* gene: three (DSC10, 12, and the SVA) in *TAF1* introns and the remaining four in the intergenic region 3' to its terminal exon (Makino et al., 2007; Nolte et al., 2003). This intergenic domain has been designated a Multiple Transcript System (MTS) based on the presence of five unconventional exons which may be transcribed as distinct RNAs and/or spliced to *TAF1*-derived transcripts (Herzfeld et al., 2007; Makino et al., 2007; Nolte et al., 2003). With the possible exception of DSC3, which falls within one of the putative MTS exons (Nolte et al., 2003), all of the XDP sequence variants appear to be non-coding, which has made their functional consequences difficult to predict. We recently derived XDP patient-specific fibroblasts and induced pluripotent stem cells (iPSCs) which were differentiated into neural stem cells (NSCs) (Ito et al., 2016). Compared to matched control cells, XDP fibroblasts and NSCs exhibited aberrant expression of some *TAF1* transcripts (Ito et al., 2016), consistent with a previous report of *TAF1* expression in XDP post-mortem striatal tissue (Makino et al., 2007). These data suggest that XDP-related sequence variants may somehow alter expression of *TAF1*, but the mechanisms underlying such alterations, as well as their downstream functional consequences, remain unclear. *TAF1* encodes TATA-Binding Protein (TBP)-Associated Factor-1 (TAF1), the largest component of the multi-subunit TFIID complex which is involved in transcription initiation by RNA polymerase II (Poll II) (Anandapadamanaban et al., 2013; Grunberg and Hahn, 2013; Malkowska et al., 2013; Papai et al., 2011; Thomas and Chiang, 2006). Given the importance of TFIID dynamics for transcription in general, it is possible that perturbations in TAF1 could potentially have broad effects on gene expression, but to date there has been little information about transcriptional patterns in XDP cells.

In this study we sought to identify functionally-related gene sets which are dysregulated in XDP cells, as such networks may offer insight into cellular pathways contributing to disease pathogenesis. Towards that end we used NanoString panels interrogating transcripts representing over thirteen canonical pathways to derive a molecular signature distinguishing XDP vs. control cells. That signature mapped strongly to nuclear factor-kappa B (NFκB), a signal transduction pathway which broadly regulates expression of genes involved in diverse functions across multiple cell types (Hayden and Ghosh, 2012; Hayden and Ghosh, 2014; Mitchell et al., 2016). NFκB signaling is mediated by monomeric subunits, p65 (RelA), RelB, cRel, p50, and p52, which at rest are retained in the cytoplasm by inhibitor of κB (IκB) proteins. Pathway activation by ligands such as tumor necrosis factor-α (TNFα) induces the IκB kinase (IKK) complex to phosphorylate IκBs, thereby releasing NFκB subunits which then dimerize in different combinations, translocate to the nucleus, and promote target gene transcription (ibid). Canonical NF-κB signaling is mediated by hetero- and homodimers of p50 and p65, and their transcriptional activity reportedly involves interactions with multiple TAFs within TFIID, including TAF1 (Amir-Zilberstein et al., 2007; Guermah et al., 1998; Schmitz et al., 1995; Silkov et al., 2002; Yamit-Hezi and Dikstein, 1998; Yamit-Hezi et al., 2000). In addition, dysregulation of NFκB signaling has been associated with a growing list of diseases, including neurodegenerative disorders such as Parkinson's (PD) and Huntington's disease (HD). Based on the signature analysis, we further characterized TNFα-induced NFκB responses in XDP vs. control fibroblasts and iPSC-differentiated NSCs. The results indicate that, compared to controls cells, patient fibroblasts and NSCs both exhibit increased NFκB activation in response to cytokine challenge, suggesting that this pathway may be an affected target in XDP.

Materials and Methods

Cell lines and culture conditions

Table 1 lists the cell lines used in this study. The initial expression profiling was performed on XDP patient fibroblast lines 32517, 33109, 33363, 33808, and 34363; and matched control fibroblast lines 32643, 33113, 33114, 33362, and 33809. The clinical characteristics of donor subjects, confirmation of XDP genotype, and derivation of fibroblasts were previously described (Ito et al., 2016). During the course of this study, four additional fibroblast lines were obtained: XDP lines 34421 and 34813, as well as control lines 33359 and 34435. Donor subjects 34421 and 34813 exhibited clinical features consistent with XDP and were confirmed to be positive for the disease haplotype, whereas the control individuals were unaffected family members who were negative for all haplotype markers. The four new lines were included in all experiments following the initial Nanostring analysis as indicated in the text, whereas fibroblast lines 33808 (XDP) and 33809 (control) were discontinued due to slower growth rates in culture which limited their propagation. All fibroblasts were cultured in Dulbecco's Modified Eagle's Medium (DMEM) supplemented with 20% fetal bovine serum and 1X Penicillin/Streptomycin/L-glutamine. Cells were passaged using trypsin.

Reprogramming of XDP (32517, 33109, 33363, 33808, and 34363) and control (33113, 33114, and 33362) fibroblasts to iPSCs and neural conversion to NSCs were previously documented (Ito et al., 2016). The nomenclature for each NSC clone relative to its parent fibroblast line is also listed in Table 1. NSCs were propagated on Geltrex™-coated cultureware in Neurobasal Medium: DMEM/F12 (1:1) with 2% PSC™ Neural Induction Supplement in a humidified incubator at 37°C with 5% CO_2 and passaged using Accutase. For NSC passaging, cells were re-

plated in medium supplemented with 5 μM ROCK inhibitor, Y-27632, which promotes cell survival. The inhibitor was removed after 24 h by complete medium exchange. All media and related reagents were obtained from Thermo Scientific (Waltham, MA USA).

RNA isolation and NanoString expression analysis

Fibroblasts were trypsinized, collected via centrifugation, flash frozen, and stored at -80°C pending nucleic acid isolation. Total RNA from cell pellets was isolated using miRNeasy™ kit with on-column DNase digestion (Qiagen, Valencia, CA USA) according to manufacturer's instructions with the following modifications: after adding QIAzol™ Lysis Reagent to cell pellets, tubes were incubated at room temperature for 1 min, vortexed for 30 sec, and incubated at room temperature for an additional 2 min. After addition of chloroform, tubes were shaken for 15 sec, incubated at room temperature for at least 40 sec to allow phase separation, shaken again for 15 sec, and incubated until phase separation before proceeding according to manufacturer's protocol. RNA concentration and integrity were assessed on an Agilent 2100 Bioanalyzer (Agilent, Santa Clara, CA USA).

RNA samples (20 ng/μL) were assayed on NanoString PanCancer® and Immunology® panels (NanoString Technologies., Seattle, WA USA) interrogating a total of 1540 transcripts including 80 reference genes. Profiling was performed on an nCounter® system at NanoString Technologies (Seattle, WA). Four biological replicates of each cell line were assayed across three independent trials.

Initial pre-processing of raw NanoString counts and marker gene selection were performed using nSolver 2.0™ software. Data pre-processing included (1) subtraction of background fluorescence as determined by negative (H_2O) control samples; and (2) normalization of fluorescence counts to positive controls to account for differences in probe hybridization efficiency. All but two of the reference genes displayed stable counts in XDP and control samples across all experiments. Counts for each target RNA were normalized to the geometric mean of 78 reference genes, and normalized data were used to identify marker genes distinguishing XDP from control cells at $p < 0.05$. Pathway analysis of the resulting signature was performed using Ingenuity® Pathway Analysis (IPA) software (Qiagen).

Quantitative RT-PCR for NFκB target genes

RNA isolated from XDP and control lines was reverse transcribed into cDNA using RT^2 First Strand Kit with additional DNase digestion to remove any residual contaminating genomic DNA (Qiagen). Expression of some NFκB target genes was quantified in individual reactions using Taqman® primers and probes (Thermo Scientific) on a StepOne Plus™ Real-Time PCR System (Applied Biosystems) as recommended. Each reaction assayed 82 ng RNA in 20 µL total volume for an initial holding step for 95°C (20 sec) followed by 40 cycles of 95°C (1 sec) and 60°C (20 sec). Raw Ct values for each target gene were normalized to the geometric mean of reference genes, *GUSB* and *UBC*. To quantify expression of a broader range of NFκB genes, RNA was also analyzed using RT^2 Profiler™ PCR Arrays interrogating 84 known NFκB signaling targets (Qiagen, Cat# PAHS-225Z) based on SYBR Green detection. For these reactions, 1 µg of total RNA was used per cell line per 96-well array and assayed on a BioRad CFX-96™ instrument with the following run conditions: 95°C (10 min) followed by 40 cycles of

95°C (15 sec) and 60°C (60 sec) at a ramp rate of 1°C/sec. Raw Ct values for each target gene were normalized to the geometric mean of reference genes, *ACTB*, *GAPDH*, *HPRT1*, and *RPLP0*.

NFκB-luciferase reporter assay

Fibroblasts and NSCs were infected with a lentivirus encoding the secreted *Gaussia* luciferase (GLuc) under the transcriptional control of a minimal promoter bearing five tandem repeats of the NFκB response element (Badr et al., 2009). Cells were inoculated with virus diluted to an approximate multiplicity of infection (M.O.I.) of 50 in culture medium supplemented with 10 µM polybrene. Media was changed 24 h later. For fibroblasts, cells were batch-infected in 6-well plates, collected on day 2, resuspended in DMEM with reduced serum (0.5%) and reseeded into triplicate wells in 96-well assay plates. Because passaging of NSCs requires ROCK inhibitor which might modulate NFκB activity, cells were seeded directly into 96-well assay plates and infected with the lentivirus reporter construct 24 h after the inhibitor was removed by medium exchange. For each cell line, mock infected cells were included as a negative control. Fibroblasts and NSCs were assayed on day 3 post-infection. Prior to stimulation, 10 µL aliquots were sampled from each well and mixed with the GLuc-specific substrate, coelenterazine (Nanolight Technology; Pinetop, AZ USA), at a final concentration of 1.67 µg/mL. Baseline relative light units (RLU) were measured on a Synergy HTX™ luminometer (Biotek, Winooski, VT) using a 1 sec integration time. Cells were then stimulated with decreasing amounts of recombinant human TNFα (R&D systems) to achieve final concentrations of 100 - 0.1 ng/mL. Control cells were mock-stimulated with an equivalent volume of media only. At 4 h post-stimulation, media was sampled and assayed for GLuc activity as before. RLU values measured

in GLuc reporter-infected cells were adjusted for background luciferase activity based on counts measured in corresponding mock-infected cells. Adjusted RLU values were used to calculate the increase in GLuc relative to baseline for each individual well. The fold change in GLuc activity relative to untreated cells was calculated for each concentration of TNFα to generate dose-response curves for each cell line. Each cell line was assayed in at least three independent trials, and results were averaged to generate mean dose-response profiles for XDP vs. control fibroblasts and NSCs.

SDS-PAGE and western blot analysis

Cells were collected by scraping and centrifugation, then washed 3X in cold phosphate-buffered saline (PBS) prior to lysis in RIPA buffer (150 mM NaCl, 50 mM Tris pH 7.5, 1% Nonidet P-40, 0.5% deoxycholate, 0.1% SDS) with 1X protease inhibitor (Complete Mini™; Roche, Indianapolis, IN USA). 25 µg total protein from each lysate were prepared in Novex Bolt™ lithium dodecyl sulfate (LDS) sample buffer, resolved by electrophoresis on Novex Bolt™ bis-acrylamide (4-12%) gels and transferred to polyvinylidene fluoride (PVDF) membranes (all from Thermo Scientific). Membranes were blocked with 0.5% milk in TBS-T (150 mM NaCl, 50 mM Tris pH 7.9, 0.5% TWEEN) and incubated overnight in primary antibodies diluted in 0.5% milk in TBS-T. Blots were washed 3X in TBS-T and incubated in HRP-conjugated secondary antibodies, with labeled proteins visualized via chemiluminescence using SuperSignal West Pico Substrate™ (Thermo Scientific). Intensity values for immunoreactive bands were determined by densitometry using ImageJ software (Schneider et al., 2012).

Antibodies and dilutions used for western blotting were: rabbit anti-NFκB p65 (sc-372; 1:100; Santa Cruz Biotechnology, Santa Cruz, CA USA); rabbit anti- NFκB p105:p50 (ab32360; 1:400; Abcam; Cambridge, MA USA); mouse anti-Hsp70 (sc-24; 1:6,000; Santa Cruz); mouse anti-GAPDH (MAB374; 1:10,000; Millipore, Billerica, MA USA); rabbit anti-histone H3 (9715; 1:10,000; Cell Signaling; Danvers, MA USA); HRP-conjugated anti-rabbit and –mouse IgG (NA934 and NA931; 1:10,000; GE Life Sciences, Pittsburgh, PA USA).

DNA binding ELISA for NFκB subunits

As an alternative to an electrophoretic mobility shift assay, an enzyme-linked immunosorbent assay (ELISA)-type format (TransAM®; Active Motif; Carlsbad, CA USA) was used to quantify DNA binding of activated NFκB p50 and p65 subunits. The assay was performed in 96-well plates in which an oligonucleotide bearing the NFκB DNA consensus sequence was immobilized. Fibroblasts or NSCs were stimulated with 1 ng/mL TNFα or medium only in DMEM containing 0.5% Fetal Bovine Serum (FBS) (fibroblasts) or neural expansion medium (NSCs), then lysed. Equivalent amounts of total protein were incubated in duplicate wells as recommended. Captured p50 or p65 was detected via HRP-labeled specific antibodies, visualized by reaction with HRP substrate, and quantified by spectrophotometry with absorbance readings taken at 455 and 655 nm. Positive control wells contained lysate with known quantities of p50 and p65 (Active Motif). Negative control wells were spiked with one of two competitor oligonucleotides, one bearing the NFκB consensus sequence and one with a scrambled sequence to probe specificity of protein capture. For each well containing protein, optical density (O.D.) readings at 455 nm O.D. values were corrected for background signal based on readings taken at 655 nm and the signal detected in blank wells. Corrected O.D. values for each sample were

expressed as ratios relative to the internal positive control sample. Replicate samples were analyzed across at least three independent trials.

Cell Viability

Cell viability in TNFα-stimulated cells was assayed using CellTiter-Glo® (Promega). Fibroblasts and NSCs were seeded into triplicate wells of 96-well assay plates, stimulated with TNFα as indicated in the experiment, and cellular ATP levels were quantified via CellTiter-Glo® as recommended. Relative light units (RLU) were measured on a Synergy HTX™ luminometer (Biotek, Winooski, VT) using a 1 sec integration time.

Immunofluorescence

Immunostaining of NSCs was performed as previously described (Ito et al., 2016). Briefly, NSCs were fixed in 4% paraformaldehyde for 20 min at room temperature, washed in PBS, permeabilized in 0.1% Nonidet P-40 for 20 min, and then blocked in 10% normal goat serum in PBS for 1 h. Cells were incubated overnight at 4°C in primary antibodies diluted in blocking buffer, washed 3X in PBS, and then reacted with fluorophore-conjugated secondary antibodies for 1 h to visualize labeled target antigens. Cells were washed again in PBS and counterstained with Topro-3-iodide to visualize nuclei. Images were acquired using a Zeiss Axiovert 200M laser confocal microscope and Zeiss LSM 5 Pascal (v 3.2 SP2) software with sequential scanning, a frame average of 4 per channel, and a final magnification of 100X. Antibodies and dilutions used for immunostaining were: mouse anti-nestin (ab21628; 1:200; Abcam); rabbit anti-Musashi (ab21628; 1:100; Abcam); rabbit anti-Sox1 (ab87775; 1:250; Abcam); Alexa

Fluor®488-conjugated anti-rabbit IgG (A-11008; 1:1000; Thermo Scientific); Alexa Fluor®594-conjugated anti-mouse IgG (A-11032; 1:1000; Thermo Scientific).

Statistical analyses

RT-PCR gene expression data were analyzed using RT^2 Profiler™ PCR Array Data Analysis software v. 3.5 (Qiagen) to calculate *p* values based on Student's t-tests of replicate $2^{-\Delta Ct}$ values for each comparison. Two-way Analysis of Variance (ANOVA) and Chi-square analysis were performed with GraphPad Prism® 7 software (GraphPad Software; La Jolla, CA USA). Heatmaps of gene expression data were generated using GENE-E (Broad Institute; Cambridge, MA USA).

Results

An XDP molecular signature maps to networks related to NFκB and RNA polymerase II

NanoString technology was used to identify gene sets differentially regulated in XDP vs. control fibroblasts as it enables rapid, multiplexed quantification of up to 800 transcripts within a single sample (Geiss et al., 2008). The patient fibroblast lines were derived from individuals displaying clinical features consistent with XDP and confirmed to be positive for six of the known haplotype markers (the SVA and five DSCs), whereas the control fibroblasts were obtained from unaffected family members confirmed to be haplotype-negative (Ito et al., 2016). RNA from replicate XDP and control fibroblast lines (n = 5 each) was assayed on two panels interrogating 1540 transcripts representing a broad range of cellular pathways. That analysis identified a 51-gene signature distinguishing XDP vs. control fibroblasts at $p < 0.05$ (Figure 1). The top three

signature genes, *CXCL2*, *IL8*, and *TNFAIP6*, which showed the greatest downregulation in XDP vs. control fibroblasts, were separately confirmed by real-time PCR with Taqman primers from independent samples. Fold changes for each gene obtained by real-time PCR were slightly lower than those calculated by NanoString (Table 2), which may be due to the fact that the latter quantifies target transcripts without an amplification step (Geiss et al., 2008).

We hypothesized that the XDP signature would include gene sets specifically linked to TFIID and/or RNA polymerase II (Pol II), given their known relationships to TAF1 and our previous observations of aberrant *TAF1* expression in XDP fibroblasts (Ito et al., 2016). Consistent with that hypothesis, Ingenuity® Pathway Analysis (IPA®) revealed significant overlap between the XDP signature and networks linked to Pol II (Table 3 and Figure 2A), including the androgen receptor (*AR*) and p53 (*TP53*), both of which have been shown to directly interact with TAF1 (Cai and Liu, 2008; Li et al., 2004; Tavassoli et al., 2010; Wu et al., 2014). That analysis further revealed even greater overlap with genes known to be regulated by inflammatory mediators, specifically: the bacterial endotoxin, lipopolysaccharide (LPS); cytokines TNFα, interferon-γ (IFNγ), and interleukin-1β; Toll-like receptors (TLRs); and components of the NFκB pathway (Table 3 and Figure 2B). LPS, pro-inflammatory cytokines, and activation of TLRs are all known to induce signaling via NFκB, suggesting that these observations may represent a common cascade.

XDP fibroblasts exhibit increased NFκB-luciferase activity in response to TNFα

Because NFκB and related inflammatory molecules had not been previously implicated in XDP, we further characterized this signaling phenotype in XDP vs. control cell lines. The NanoString

signature indicated that constitutive NFκB activity was decreased in XDP vs. control fibroblasts, as suggested by the significant downregulation observed in known NFκB target genes, *CXCL2, IL8,* and *TNFAIP6*. To compare cytokine-evoked NFκB activity in XDP vs. control cells, we first used a luciferase reporter assay to screen concentrations of TNFα which induce NFκB responses in these cell lines. The reporter construct was based on the secreted GLuc protein (Badr et al., 2009) which can be assayed in conditioned media from live cells, facilitating pre- and post-stimulation measurements from the same well. Thus each well served as its own baseline control, thereby accounting for any well-to-well differences in the number of transduced cells. Because the NFκB-luciferase reporter lacked a fluorescent marker, in parallel we separately infected all fibroblast lines with a lentivirus vector encoding GFP driven by a strong viral promoter and quantified infection efficiency by flow cytometry. All cell lines showed comparable infection efficiencies, based on percent GFP expression (Supplemental Figure 1). In initial experiments with the NFκB-luciferase reporter, we noted that TNFα responses were more variable in fibroblasts cultured in normal growth medium containing 20% serum. This variability decreased when cells were switched to medium containing reduced serum (0.5%) just prior to analysis. For that reason all measurements of TNFα responses were performed under these conditions.

Although the transcriptional profiling performed in unstimulated fibroblasts suggested that constitutive NFκB was decreased in XDP vs. control cells, the luciferase reporter assay revealed the opposite pattern in response to cytokine challenge. Compared to control cells, XDP fibroblasts exhibited increased NFκB-luciferase activity induced by TNFα (Figure 3). Two-way

ANOVA of the dose-response curves revealed significant effects for genotype ($p < 0.0001$) and TNFα treatment ($p < 0.0001$), although the interaction did not reach significance.

Decreased activation of the NFκB p50 subunit in XDP vs. control fibroblasts

Based on the results of the luciferase reporter assay, we chose a single concentration of TNFα to examine temporal NFκB dynamics by measuring production of the active (i.e. DNA-binding) forms of the p50 and p65 subunits. Prior to that, we used western blotting of whole cell lysates to first confirm detection of endogenous p50 and p65 and probe for any genotypic differences in total protein expression at baseline (Figure 4). Both proteins were detected in all cell lines, including the precursor protein, p105, from which the p50 subunit is generated by proteolytic processing. Although some variability was noted across the cell lines, there were no significant genotypic differences in total p50 or p65 levels.

We then assayed generation of the active forms of each subunit using an ELISA-type assay in which the proteins were captured by an immobilized oligonucleotide bearing the NFκB consensus sequence, with detection and quantification achieved with specific antibodies. Lysates were prepared from XDP and control fibroblasts stimulated with 1 ng/mL TNFα for increasing time intervals over a 90-min time course, as well as unstimulated control cultures. For both genotypes, DNA-bound p50 began to increase above baseline by 10 min post-stimulation, achieved peak levels at 30-45 min, and remained elevated at 90 min (Figure 5A). However, both basal and peak levels of DNA-bound p50 were lower in XDP lysates than in control samples. Two-way ANOVA of the p50 activation profiles revealed significant effects for genotype ($p < 0.001$) and TNFα treatment ($p < 0.001$) though not for the interaction. In contrast,

activation of the p65 subunit did not differ significantly in XDP vs. control lysates (Figure 5B). For both p50 and p65, the increased signal in lysates from stimulated cells could be blocked by spiking in the wild-type, but not scrambled, competitor oligonucleotide, confirming specificity of the assays (data not shown).

Because cytokine stimulation of cultured cells can induce toxicity, we assayed cell viability in parallel by quantifying cellular ATP levels in XDP vs. control fibroblasts challenged with TNFα for the same intervals used to monitor NFκB subunit dynamics. We found no significant differences in cell viability after stimulation or between genotypes (Supplemental Figure 2A).

Expression of endogenous NFκB target genes is increased in XDP vs. control fibroblasts stimulated with TNFα.

Expression of the top three signature genes, *CXCL2, IL8,* and *TNFAIP6,* was then assayed in XDP and control fibroblasts challenged with 1 ng/mL TNFα for either 60 or 90 min versus mock-stimulation with media alone. Although constitutive expression of all three genes was decreased in XDP vs. control fibroblasts (Table 2), the level of TNFα-induced expression was increased in patient cells compared to controls (Figure 6). For both *IL8* and *TNFAIP6,* the levels induced by 90 min stimulation with TNFα differed significantly in XDP vs. control, although the difference observed for *CXCL2* was more modest. Nevertheless, the pattern appeared consistent with the results of the luciferase reporter assay, indicating that XDP fibroblasts appear hypersensitive to a pro-inflammatory cytokine challenge.

NFκB-luciferase reporter activity is also increased in XDP vs. control neural stem cells

Having detected differential NFκB responses in XDP vs. control fibroblasts, we next examined whether the signaling phenotype was maintained following reprogramming to iPSCs and conversion to NSCs. Five XDP fibroblast lines and three control lines were recently used to generate seven XDP and six control iPSC clones, respectively, which were all differentiated into NSCs (Ito et al., 2016) (Table 1). Tri-lineage potential of iPSC clones, neural conversion to NSCs, and inter-NSC clone variability of neural stem cell marker expression were all previously documented (ibid). Supplemental Figure 3 depicts representative XDP and control NSC clones with similar expression of Nestin, Musashi, and Sox1.

XDP and control NSCs exhibited the same pattern in the NFκB-luciferase reporter assay as was observed in the fibroblast lines. The XDP clones had increased responses to TNFα than did control NSCs (Figure 7A). Two-way ANOVA of the NSC dose-response curves revealed significant effects for genotype ($p < 0.001$) and TNFα treatment ($p < 0.001$) but not for the interaction. Yet unlike the fibroblast lines, the NSC clones did not exhibit genotypic differences in the generation of the active NFκB subunits based on the ELISA-DNA binding assay. Following stimulation with 1 ng/mL TNFα, levels of DNA-bound p50 and p65 increased robustly above baseline over time, with peak levels at 30 min, confirming endogenous pathway activation in the NSCs, but the fold induction was equivalent between XDP and control clones (Figure 7B, C). As was performed with fibroblasts, we verified that stimulation with TNFα over a 90 min time course did not induce any significant cell death in either XDP or control clones (Supplemental Figure 2B).

Increased expression of NFκB target genes in XDP vs. control neural stem cells

To more broadly compare expression of endogenous NFκB-responsive genes in XDP vs. control NSC clones, we used PCR arrays interrogating 84 known targets to assay TNFα–induced transcription in these cell lines. Figure 8 provides a heatmap depicting both basal and induced expression of each gene target in each NSC clone. For the 84 transcripts measured, the rank order of fold induction above baseline was largely similar across all clones. With few exceptions, the average fold increase induced by TNFα for each gene was higher in XDP clones than in controls, but none of the differences in individual means achieved significance based on Student's t-test with correction for multiple hypothesis testing. In general, the genes which appeared to be most sensitive to TNFα, based on robust induction of 10-fold or greater in XDP clones, also showed the greatest variability in expression across all cell lines. The most striking difference between the genotypes appeared to be in genes which were less sensitive to TNFα. In the control arrays, 29 of 84 genes (34.5%) showed no response to TNFα, in contrast to the XDP arrays in which all but 3 genes (3.6%) showed at least low level induction due to cytokine treatment (Figure 9). Chi-square analysis revealed a significant difference in the distribution of fold change values between XDP and control NSCs (X^2= 26.3, df = 3, $p < 0.0001$), further suggesting that the patient NSCs respond to cytokine challenge with a broader activation of NFκB target genes than do corresponding control cells.

Discussion

Since the description of the first reported cases (Lee et al., 1976), most research into XDP has focused on detailed characterizations of the clinical phenotype (Aguilar et al., 2011; Evidente et al., 2002a; Evidente et al., 2002b; Evidente et al., 2004; Jamora et al., 2014; Lee et al., 1991; Lee et al., 2002; Lee et al., 2011; Pasco et al., 2011) and efforts to pinpoint the pathogenic gene

lesion (Domingo et al., 2015; Graeber and Muller, 1992; Haberhausen et al., 1995; Herzfeld et al., 2007; Kupke et al., 1992; Makino et al., 2007; Muller et al., 1994; Nemeth et al., 1999; Nolte et al., 2003; Wilhelmsen et al., 1991). There have been limited analyses of post-mortem brain tissue which have described XDP-related neuropathology (Goto et al., 2013; Goto et al., 2005; Waters et al., 1993) and expression of certain transcripts within the striatum (Makino et al., 2007), but to date there has been little information about specific cellular defects which might contribute to disease pathogenesis. This gap in knowledge has no doubt been exacerbated by the challenges in understanding the genetics of XDP. The cases documented so far have all suggested that the seven known XDP haplotype markers in and around *TAF1* are consistently inherited together, which has made it difficult to determine which, if any, of these sequence variants may be driving the disease process (Domingo et al., 2015; Makino et al., 2007; Nolte et al., 2003). Our recent demonstration that *TAF1* transcript expression is altered in XDP vs. control fibroblasts and NSCs supports the hypothesis that a functional defect in TAF1 could somehow contribute to XDP pathogenesis (Ito et al., 2016), but the nature of that defect is still unclear. For that reason, our strategy for seeking cellular pathways affected in XDP cells began with transcriptional profiling of defined gene sets, as this approach did not require *a priori* knowledge of the pathogenic gene variant.

The results revealed aberrant NFκB signaling in both XDP fibroblasts and NSCs, though some differences were noted. Compared to control cells, XDP fibroblasts exhibited decreased constitutive NFκB activity and levels of active p50, yet increased responses to TNFα. A similar pattern was reported in p50-null mice, in which constitutive NFκB-related gene expression was decreased but cytokine-evoked responses were increased (Driessler et al., 2004). The reduced

basal expression in these mice most likely reflected the requirement for p50/p65 heterodimers in constitutive NFκB transcription (Hinata et al., 2003). Furthermore, because the p50 subunit lacks a transactivation domain and by itself functions as a transcriptional repressor (Kaltschmidt et al., 2005), its absence during evoked NFκB activity can lead to enhanced transcription. While our observations of XDP fibroblasts appear consistent with the description of p50-null mice, we also observed increased TNFα responses in XDP vs. control NSCs, even though p50 levels and constitutive pathway activity did not vary by genotype. Thus the data suggest that hypersensitivity to TNFα may be a common phenotype in both cell types, but the mechanism underlying the dysregulation has not been determined.

NFκB is one of the most extensively characterized signal transduction pathways which coordinates the expression of at least 500 known target genes involved in a broad array of cellular functions across diverse cell types (for review, see (Hayden and Ghosh, 2012; Hayden and Ghosh, 2014; Mitchell et al., 2016). In neurons, NFκB subunits are localized at the synapse, with pathway activation resulting in retrograde trafficking, nuclear translocation, and modulation of target gene expression (Meffert et al., 2003; Mikenberg et al., 2007; Salles et al., 2014; Shrum et al., 2009). These NFκB-related transcriptional networks may be induced by numerous synaptic stimuli and have been shown to play critical roles in both neurodevelopment and adult plasticity (Boersma et al., 2011; Engelmann and Haenold, 2016; Kaltschmidt and Kaltschmidt, 2009; Mattson and Meffert, 2006; Meffert and Baltimore, 2005). Furthermore, an increasing number of neurologic disorders has been associated with either hypo- or hyperactive NFκB signaling in neurons and glia, illustrating how this pathway may regulate both cell death- and survival-related responses in different cell types (Crampton and O'Keeffe, 2013; Mattson, 2006;

Schmidt-Ullrich et al., 1996; Snow et al., 2014; Srinivasan and Lahiri, 2015). In these syndromes, there has been considerable emphasis on the role of astrocytes and microglia, in which increased NFκB activity induces the release of potentially toxic factors, including cytokines, chemokines, prostaglandins, and complement proteins (Gu et al., 2015; Kaur et al., 2015; Shih et al., 2015). These pro-inflammatory molecules may damage surrounding neurons, thereby contributing to disease progression (Gao and Hong, 2008; Glass et al., 2010; Hoarau et al., 2011; Nguyen et al., 2002; Stephan et al., 2012; Wyss-Coray and Mucke, 2002).

NFκB signaling has been specifically implicated in both PD and HD, which share clinical and pathologic features, respectively, with XDP. Multiple studies have documented increased glial activation, inflammatory gene expression, and nuclear translocation of NFκB subunits in post-mortem PD brain, compared to control tissue (Hunot et al., 1997; Kim and Joh, 2006; McGeer and McGeer, 2008; Mogi et al., 2007; Nagatsu and Sawada, 2005; Tansey et al., 2007). Similar observations have been made in HD brain tissue, patient cell lines, and transgenic mouse models (Bjorkqvist et al., 2008; Hsiao et al., 2013; Sapp et al., 2001; Tai et al., 2007; Trager et al., 2014). Moreover, NFκB signaling may be regulated by proteins implicated in PD and HD, specifically: huntingtin, DJ-1, PTEN-induced putative kinase-1 (PINK1), parkin, leucine-rich repeat kinase-2 (LRRK2), and α-synuclein. PINK1 and DJ-1 each bind related proteins, TNF receptor-associated factor-6 (TRAF6) and Cezanne, respectively, which are involved in upstream NFκB signal transduction, whereas parkin ubiquitinates TNF receptor-associated factor-2 (TRAF2) and IKK-γ (Henn et al., 2007; Lee et al., 2012; McNally et al., 2011; Muller-Rischart et al., 2013; Sha et al., 2010). Huntingtin also binds IKK-γ (Khoshnan et al., 2004) and in neurons mediates retrograde transport of NFκB subunits from the synapse to cell body (Marcora

and Kennedy, 2010). All of these interactions enhance NFκB pathway activity. Overexpression or knockdown of LRRK2 appears to enhance or attenuate, respectively, inflammatory gene expression (Gardet et al., 2010; Kim et al., 2012; Lopez de Maturana et al., 2014; Moehle et al., 2012), which may be due to its effects on nuclear translocation of the NFκB p50 subunit (Russo et al., 2015). In glial cells, LRRK2 depletion also diminishes NFκB signaling in response to α-synuclein, which binds Toll-like receptors (Daniele et al., 2015; Fellner et al., 2013; Kim et al., 2013; Russo et al., 2015; Watson et al., 2012). Collectively these complex relationships illustrate how seemingly disparate proteins involved in PD and HD may share common relationships to NFκB.

Unlike PD and HD, XDP has not yet been associated with neuroinflammation. The previous neuropathological studies noted that the disease-related dropout of medium spiny neurons in striatum was accompanied by increased astrogliosis (Goto et al., 2013; Goto et al., 2005), but specific markers of inflammation, as well as microglia status, were not evaluated. In addition, the relationship between NFκB and TAF1, the protein most strongly linked to XDP based on current evidence, is less well defined than with PD- and HD-related proteins. Previous studies have shown that a coding point mutation in TAF1 in the hamster cell line, ts13, is associated with defective NFκB signaling, although the mechanism was not defined (Amir-Zilberstein et al., 2007). Other reports indicate that TFIID may act as a bridge between the general transcription machinery and gene-specific activators like NFκB, and within this complex the NFκB p65 subunit interacts directly with multiple TAFs, including TAF1 (Guermah et al., 1998; Silkov et al., 2002; Yamit-Hezi and Dikstein, 1998; Yamit-Hezi et al., 2000). Based on these data, it is possible that interactions between TAF1 and NFκB subunits somehow modulate NFκB-related

gene expression, with perturbations in TAF1 resulting in altered NFκB transcriptional output. The observations that XDP fibroblasts and iPSC-derived NSCs display both an NFκB phenotype (this study) as well as altered expression of *TAF1*-derived transcripts (Domingo et al., 2016; Ito et al., 2016) could be consistent with that possibility. However, further study is required to fully determine how XDP-related sequence variants affect TAF1 protein isoforms, how these TAF1 species interact with NFκB signaling components, and how such interactions might mechanistically influence the transcriptional output of this pathway.

A caveat of this study is that the transcriptional profiling which identified differential expression of NFκB-related gene sets was based on panels interrogating a limited set of cellular pathways. Thus in these analyses, pathway discovery was restricted to gene sets represented in these arrays. Future studies based on genomewide RNA sequencing of XDP model cell lines may no doubt uncover additional transcriptional phenotypes which may also be relevant to disease pathogenesis. Nevertheless, the data presented here provide initial evidence of an XDP-related cellular phenotype involving NFκB, a pathway already associated with other neurodegenerative disorders which share overlapping clinical and/or pathologic features. Given the potential link to these other disorders, as well as the numerous compounds targeting the NFκB pathway in various stages of therapeutics development (Arepalli et al., 2015; Gilmore and Herscovitch, 2006; Gupta et al., 2010; Miller et al., 2010), further characterization of NFκB dynamics in XDP model systems may be warranted.

Acknowledgements

The authors gratefully acknowledge Dr. Errol Rueckert (Nanostring Technologies) for assistance with transcriptional profiling, and Dr. Alain Viel (Harvard University) for assistance with qPCR arrays. Funding for this study was provided by the MGH Collaborative Center for X-Linked Dystonia-Parkinsonism (DCB, NS) and NIH P01 NS087997 (DCB, NS).

References

Aguilar, J. A., et al., 2011. The promise of deep brain stimulation in X-linked dystonia parkinsonism. Int J Neurosci. 121 Suppl 1**,** 57-63.

Amir-Zilberstein, L., et al., 2007. Differential regulation of NF-kappaB by elongation factors is determined by core promoter type. Mol Cell Biol. 27**,** 5246-59.

Anandapadamanaban, M., et al., 2013. High-resolution structure of TBP with TAF1 reveals anchoring patterns in transcriptional regulation. Nat Struct Mol Biol. 20**,** 1008-14.

Arepalli, S. K., et al., 2015. Novel NF-kappaB inhibitors: a patent review (2011 - 2014). Expert Opin Ther Pat. 25**,** 319-34.

Badr, C. E., et al., 2009. Real-time monitoring of nuclear factor kappaB activity in cultured cells and in animal models. Mol Imaging. 8**,** 278-90.

Bjorkqvist, M., et al., 2008. A novel pathogenic pathway of immune activation detectable before clinical onset in Huntington's disease. J Exp Med. 205**,** 1869-77.

Boersma, M. C., et al., 2011. A requirement for nuclear factor-kappaB in developmental and plasticity-associated synaptogenesis. J Neurosci. 31**,** 5414-25.

Cai, X., Liu, X., 2008. Inhibition of Thr-55 phosphorylation restores p53 nuclear localization and sensitizes cancer cells to DNA damage. Proc Natl Acad Sci U S A. 105**,** 16958-63.

Crampton, S. J., O'Keeffe, G. W., 2013. NF-kappaB: emerging roles in hippocampal development and function. Int J Biochem Cell Biol. 45**,** 1821-4.

Daniele, S. G., et al., 2015. Activation of MyD88-dependent TLR1/2 signaling by misfolded alpha-synuclein, a protein linked to neurodegenerative disorders. Sci Signal. 8**,** ra45.

Domingo, A., et al., 2016. Evidence of TAF1 dysfunction in peripheral models of X-linked dystonia-parkinsonism. Cell Mol Life Sci. 73**,** 3205-15.

Domingo, A., et al., 2015. New insights into the genetics of X-linked dystonia-parkinsonism (XDP, DYT3). Eur J Hum Genet. 23**,** 1334-40.

Driessler, F., et al., 2004. Molecular mechanisms of interleukin-10-mediated inhibition of NF-kappaB activity: a role for p50. Clin Exp Immunol. 135**,** 64-73.

Engelmann, C., Haenold, R., 2016. Transcriptional Control of Synaptic Plasticity by Transcription Factor NF-kappaB. Neural Plast. 2016**,** 7027949.

Evidente, V. G., et al., 2002a. Phenomenology of "Lubag" or X-linked dystonia-parkinsonism. Mov Disord. 17**,** 1271-7.

Evidente, V. G., et al., 2002b. X-linked dystonia ("Lubag") presenting predominantly with parkinsonism: a more benign phenotype? Mov Disord. 17**,** 200-2.

Evidente, V. G., et al., 2004. Phenotypic and molecular analyses of X-linked dystonia-parkinsonism ("lubag") in women. Arch Neurol. 61**,** 1956-9.

Fellner, L., et al., 2013. Toll-like receptor 4 is required for alpha-synuclein dependent activation of microglia and astroglia. Glia. 61**,** 349-60.

Gao, H. M., Hong, J. S., 2008. Why neurodegenerative diseases are progressive: uncontrolled inflammation drives disease progression. Trends Immunol. 29**,** 357-65.

Gardet, A., et al., 2010. LRRK2 is involved in the IFN-gamma response and host response to pathogens. J Immunol. 185**,** 5577-85.

Geiss, G. K., et al., 2008. Direct multiplexed measurement of gene expression with color-coded probe pairs. Nat Biotechnol. 26**,** 317-25.

Gilmore, T. D., Herscovitch, M., 2006. Inhibitors of NF-kappaB signaling: 785 and counting. Oncogene. 25**,** 6887-99.

Glass, C. K., et al., 2010. Mechanisms underlying inflammation in neurodegeneration. Cell. 140**,** 918-34.

Goto, S., et al., 2013. Defects in the striatal neuropeptide Y system in X-linked dystonia-parkinsonism. Brain. 136**,** 1555-67.

Goto, S., et al., 2005. Functional anatomy of the basal ganglia in X-linked recessive dystonia-parkinsonism. Ann Neurol. 58**,** 7-17.

Graeber, M. B., Muller, U., 1992. The X-linked dystonia-parkinsonism syndrome (XDP): clinical and molecular genetic analysis. Brain Pathol. 2**,** 287-95.

Grunberg, S., Hahn, S., 2013. Structural insights into transcription initiation by RNA polymerase II. Trends Biochem Sci. 38**,** 603-11.

Gu, Y., et al., 2015. Role of TNF in mast cell neuroinflammation and pain. J Biol Regul Homeost Agents. 29**,** 787-91.

Guermah, M., et al., 1998. Involvement of TFIID and USA components in transcriptional activation of the human immunodeficiency virus promoter by NF-kappaB and Sp1. Mol Cell Biol. 18**,** 3234-44.

Gupta, S. C., et al., 2010. Inhibiting NF-kappaB activation by small molecules as a therapeutic strategy. Biochim Biophys Acta. 1799**,** 775-87.

Haberhausen, G., et al., 1995. Assignment of the dystonia-parkinsonism syndrome locus, DYT3, to a small region within a 1.8-Mb YAC contig of Xq13.1. Am J Hum Genet. 57**,** 644-50.

Hayden, M. S., Ghosh, S., 2012. NF-kappaB, the first quarter-century: remarkable progress and outstanding questions. Genes Dev. 26**,** 203-34.

Hayden, M. S., Ghosh, S., 2014. Regulation of NF-kappaB by TNF family cytokines. Semin Immunol. 26**,** 253-66.

Henn, I. H., et al., 2007. Parkin mediates neuroprotection through activation of IkappaB kinase/nuclear factor-kappaB signaling. J Neurosci. 27**,** 1868-78.

Herzfeld, T., et al., 2007. Structural and functional analysis of the human TAF1/DYT3 multiple transcript system. Mamm Genome. 18**,** 787-95.

Hinata, K., et al., 2003. Divergent gene regulation and growth effects by NF-kappa B in epithelial and mesenchymal cells of human skin. Oncogene. 22**,** 1955-64.

Hoarau, J. J., et al., 2011. Activation and control of CNS innate immune responses in health and diseases: a balancing act finely tuned by neuroimmune regulators (NIReg). CNS Neurol Disord Drug Targets. 10**,** 25-43.

Hsiao, H. Y., et al., 2013. A critical role of astrocyte-mediated nuclear factor-kappaB-dependent inflammation in Huntington's disease. Hum Mol Genet. 22**,** 1826-42.

Hunot, S., et al., 1997. Nuclear translocation of NF-kappaB is increased in dopaminergic neurons of patients with parkinson disease. Proc Natl Acad Sci U S A. 94**,** 7531-6.

Ito, N., et al., 2016. Decreased N-TAF1 expression in X-Linked Dystonia-Parkinsonism patient-specific neural stem cells. Dis Model Mech.

Jamora, R. D., et al., 2014. Nonmotor features in sex-linked dystonia parkinsonism. Neurodegener Dis Manag. 4**,** 283-9.

Kaltschmidt, B., Kaltschmidt, C., 2009. NF-kappaB in the nervous system. Cold Spring Harb Perspect Biol. 1**,** a001271.

Kaltschmidt, B., et al., 2005. Signaling via NF-kappaB in the nervous system. Biochim Biophys Acta. 1745**,** 287-99.

Kaur, U., et al., 2015. Reactive oxygen species, redox signaling and neuroinflammation in Alzheimer's disease: the NF-kappaB connection. Curr Top Med Chem. 15**,** 446-57.

Khoshnan, A., et al., 2004. Activation of the IkappaB kinase complex and nuclear factor-kappaB contributes to mutant huntingtin neurotoxicity. J Neurosci. 24**,** 7999-8008.

Kim, B., et al., 2012. Impaired inflammatory responses in murine Lrrk2-knockdown brain microglia. PLoS One. 7**,** e34693.

Kim, C., et al., 2013. Neuron-released oligomeric alpha-synuclein is an endogenous agonist of TLR2 for paracrine activation of microglia. Nat Commun. 4**,** 1562.

Kim, Y. S., Joh, T. H., 2006. Microglia, major player in the brain inflammation: their roles in the pathogenesis of Parkinson's disease. Exp Mol Med. 38**,** 333-47.

Kupke, K. G., et al., 1992. Dystonia-parkinsonism syndrome (XDP) locus: flanking markers in Xq12-q21.1. Am J Hum Genet. 50**,** 808-15.

Lee, H. J., et al., 2012. PINK1 stimulates interleukin-1beta-mediated inflammatory signaling via the positive regulation of TRAF6 and TAK1. Cell Mol Life Sci. 69**,** 3301-15.

Lee, L. V., et al., 1991. The phenotype of the X-linked dystonia-parkinsonism syndrome. An assessment of 42 cases in the Philippines. Medicine (Baltimore). 70**,** 179-87.

Lee, L. V., et al., 2002. The natural history of sex-linked recessive dystonia parkinsonism of Panay, Philippines (XDP). Parkinsonism Relat Disord. 9**,** 29-38.

Lee, L. V., et al., 1976. Torsion dystonia in Panay, Philippines. Adv Neurol. 14**,** 137-51.

Lee, L. V., et al., 2011. The unique phenomenology of sex-linked dystonia parkinsonism (XDP, DYT3, "Lubag"). Int J Neurosci. 121 Suppl 1**,** 3-11.

Li, H. H., et al., 2004. Phosphorylation on Thr-55 by TAF1 mediates degradation of p53: a role for TAF1 in cell G1 progression. Mol Cell. 13**,** 867-78.

Lopez de Maturana, R., et al., 2014. Leucine-rich repeat kinase 2 modulates cyclooxygenase 2 and the inflammatory response in idiopathic and genetic Parkinson's disease. Neurobiol Aging. 35**,** 1116-24.

Makino, S., et al., 2007. Reduced neuron-specific expression of the TAF1 gene is associated with X-linked dystonia-parkinsonism. Am J Hum Genet. 80**,** 393-406.

Malkowska, M., et al., 2013. Structural bioinformatics of the general transcription factor TFIID. Biochimie. 95**,** 680-91.

Marcora, E., Kennedy, M. B., 2010. The Huntington's disease mutation impairs Huntingtin's role in the transport of NF-kappaB from the synapse to the nucleus. Hum Mol Genet. 19**,** 4373-84.

Mattson, M. P., 2006. Neuronal life-and-death signaling, apoptosis, and neurodegenerative disorders. Antioxid Redox Signal. 8**,** 1997-2006.

Mattson, M. P., Meffert, M. K., 2006. Roles for NF-kappaB in nerve cell survival, plasticity, and disease. Cell Death Differ. 13**,** 852-60.

McGeer, P. L., McGeer, E. G., 2008. Glial reactions in Parkinson's disease. Mov Disord. 23**,** 474-83.

McNally, R. S., et al., 2011. DJ-1 enhances cell survival through the binding of Cezanne, a negative regulator of NF-kappaB. J Biol Chem. 286**,** 4098-106.

Meffert, M. K., Baltimore, D., 2005. Physiological functions for brain NF-kappaB. Trends Neurosci. 28**,** 37-43.

Meffert, M. K., et al., 2003. NF-kappa B functions in synaptic signaling and behavior. Nat Neurosci. 6**,** 1072-8.

Mikenberg, I., et al., 2007. Transcription factor NF-kappaB is transported to the nucleus via cytoplasmic dynein/dynactin motor complex in hippocampal neurons. PLoS One. 2**,** e589.

Miller, S. C., et al., 2010. Identification of known drugs that act as inhibitors of NF-kappaB signaling and their mechanism of action. Biochem Pharmacol. 79**,** 1272-80.

Mitchell, S., et al., 2016. Signaling via the NFkappaB system. Wiley Interdiscip Rev Syst Biol Med. 8**,** 227-41.

Moehle, M. S., et al., 2012. LRRK2 inhibition attenuates microglial inflammatory responses. J Neurosci. 32**,** 1602-11.

Mogi, M., et al., 2007. p53 protein, interferon-gamma, and NF-kappaB levels are elevated in the parkinsonian brain. Neurosci Lett. 414**,** 94-7.

Muller-Rischart, A. K., et al., 2013. The E3 ligase parkin maintains mitochondrial integrity by increasing linear ubiquitination of NEMO. Mol Cell. 49**,** 908-21.

Muller, U., et al., 1994. DXS106 and DXS559 flank the X-linked dystonia-parkinsonism syndrome locus (DYT3). Genomics. 23**,** 114-7.

Nagatsu, T., Sawada, M., 2005. Inflammatory process in Parkinson's disease: role for cytokines. Curr Pharm Des. 11**,** 999-1016.

Nemeth, A. H., et al., 1999. Refined linkage disequilibrium and physical mapping of the gene locus for X-linked dystonia-parkinsonism (DYT3). Genomics. 60**,** 320-9.

Nguyen, M. D., et al., 2002. Innate immunity: the missing link in neuroprotection and neurodegeneration? Nat Rev Neurosci. 3**,** 216-27.

Nolte, D., et al., 2003. Specific sequence changes in multiple transcript system DYT3 are associated with X-linked dystonia parkinsonism. Proc Natl Acad Sci U S A. 100**,** 10347-52.

Papai, G., et al., 2011. New insights into the function of transcription factor TFIID from recent structural studies. Curr Opin Genet Dev. 21**,** 219-24.

Pasco, P. M., et al., 2011. Understanding XDP through imaging, pathology, and genetics. Int J Neurosci. 121 Suppl 1**,** 12-7.

Russo, I., et al., 2015. Leucine-rich repeat kinase 2 positively regulates inflammation and down-regulates NF-kappaB p50 signaling in cultured microglia cells. J Neuroinflammation. 12**,** 230.

Salles, A., et al., 2014. Synaptic NF-kappa B pathway in neuronal plasticity and memory. J Physiol Paris. 108**,** 256-62.

Sapp, E., et al., 2001. Early and progressive accumulation of reactive microglia in the Huntington disease brain. J Neuropathol Exp Neurol. 60**,** 161-72.

Schmidt-Ullrich, R., et al., 1996. NF-kappaB activity in transgenic mice: developmental regulation and tissue specificity. Development. 122**,** 2117-28.

Schmitz, M. L., et al., 1995. Interaction of the COOH-terminal transactivation domain of p65 NF-kappa B with TATA-binding protein, transcription factor IIB, and coactivators. J Biol Chem. 270**,** 7219-26.

Schneider, C. A., et al., 2012. NIH Image to ImageJ: 25 years of image analysis. Nat Methods. 9**,** 671-5.

Sha, D., et al., 2010. Phosphorylation of parkin by Parkinson disease-linked kinase PINK1 activates parkin E3 ligase function and NF-kappaB signaling. Hum Mol Genet. 19**,** 352-63.

Shih, R. H., et al., 2015. NF-kappaB Signaling Pathways in Neurological Inflammation: A Mini Review. Front Mol Neurosci. 8**,** 77.

Shrum, C. K., et al., 2009. Stimulated nuclear translocation of NF-kappaB and shuttling differentially depend on dynein and the dynactin complex. Proc Natl Acad Sci U S A. 106**,** 2647-52.

Silkov, A., et al., 2002. Enhanced apoptosis of B and T lymphocytes in TAFII105 dominant-negative transgenic mice is linked to nuclear factor-kappa B. J Biol Chem. 277**,** 17821-9.

Snow, W. M., et al., 2014. Roles for NF-kappaB and gene targets of NF-kappaB in synaptic plasticity, memory, and navigation. Mol Neurobiol. 49**,** 757-70.

Srinivasan, M., Lahiri, D. K., 2015. Significance of NF-kappaB as a pivotal therapeutic target in the neurodegenerative pathologies of Alzheimer's disease and multiple sclerosis. Expert Opin Ther Targets. 19**,** 471-87.

Stephan, A. H., et al., 2012. The complement system: an unexpected role in synaptic pruning during development and disease. Annu Rev Neurosci. 35**,** 369-89.

Tai, Y. F., et al., 2007. Microglial activation in presymptomatic Huntington's disease gene carriers. Brain. 130**,** 1759-66.

Tansey, M. G., et al., 2007. Neuroinflammatory mechanisms in Parkinson's disease: potential environmental triggers, pathways, and targets for early therapeutic intervention. Exp Neurol. 208**,** 1-25.

Tavassoli, P., et al., 2010. TAF1 differentially enhances androgen receptor transcriptional activity via its N-terminal kinase and ubiquitin-activating and -conjugating domains. Mol Endocrinol. 24**,** 696-708.

Thomas, M. C., Chiang, C. M., 2006. The general transcription machinery and general cofactors. Crit Rev Biochem Mol Biol. 41**,** 105-78.

Trager, U., et al., 2014. HTT-lowering reverses Huntington's disease immune dysfunction caused by NFkappaB pathway dysregulation. Brain. 137**,** 819-33.

Waters, C. H., et al., 1993. Neuropathology of lubag (x-linked dystonia parkinsonism). Mov Disord. 8**,** 387-90.

Watson, M. B., et al., 2012. Regionally-specific microglial activation in young mice over-expressing human wildtype alpha-synuclein. Exp Neurol. 237**,** 318-34.

Wilhelmsen, K. C., et al., 1991. Genetic mapping of "Lubag" (X-linked dystonia-parkinsonism) in a Filipino kindred to the pericentromeric region of the X chromosome. Ann Neurol. 29**,** 124-31.

Wu, Y., et al., 2014. Phosphorylation of p53 by TAF1 inactivates p53-dependent transcription in the DNA damage response. Mol Cell. 53**,** 63-74.

Wyss-Coray, T., Mucke, L., 2002. Inflammation in neurodegenerative disease--a double-edged sword. Neuron. 35**,** 419-32.

Yamit-Hezi, A., Dikstein, R., 1998. TAFII105 mediates activation of anti-apoptotic genes by NF-kappaB. EMBO J. 17**,** 5161-9.

Yamit-Hezi, A., et al., 2000. Interaction of TAFII105 with selected p65/RelA dimers is associated with activation of subset of NF-kappa B genes. J Biol Chem. 275**,** 18180-7.

Tables

XDP		Control	
Fibroblasts	**NSCs**	**Fibroblasts**	**NSCs**
32517	32517-I	33113	33113-2D
33109	33109-2B		33113-2I
33363	33363-C	33114	33114-B
	33363-D		33114-C
34363	34363-A	33362	33362-C
33808	33808-B		33362-D
	33808-D	33809	-
34813	-	32643	-
		33359	-
34421	-	34435	-

Table 1. Fibroblast lines and corresponding NSC lines.

Gene	**NanoString (FC)**	**TaqMan (FC)**
CXCL2	-6.06	-1.64
TNFAIP6	-4.35	-3.78
IL8	-4.5	-1.91

Table 2. Differential expression of the top three signature genes, *CXCL2*, *TNFAIP6* and *IL8*, in XDP vs. control fibroblasts as determined by Nanostring profiling vs. qPCR with Taqman chemistry. Values represent fold changes for each gene in XDP cells relative to controls. Nanostring counts for each gene were normalized to the geometric mean of 78 reference genes, while qPCR Ct values were normalized relative to the geometric mean of *UBC* and *GUSB.*

Regulator	***p* value**
Lipopolysaccharide (LPS)	1.50×10^{-20}
TNF	2.17×10^{-16}
IFNγ	7.35×10^{-13}
NFκB (complex)	1.36×10^{-12}
IκBα	8.29×10^{-12}
IFNβ1	1.37×10^{-11}
TLR4	4.36×10^{-11}
IFNα	1.70×10^{-10}
IL-1β	1.41×10^{-09}
IL-4	5.74×10^{-09}
NFκB p50	2.98×10^{-08}
NFκB p65	9.78×10^{-07}
RNA Pol II	1.19×10^{-06}

Table 3. Overlap between XDP signature and genes regulated by factors involved in inflammatory signaling/NFκB as well as RNA Pol II, as determined by IPA® pathway analysis.

Figure legends

Figure 1 (2 column width). Nanostring profiling of 1540 transcripts in XDP and control fibroblasts (n = 5 each) derived a 51-gene signature distinguishing the two genotypes at $p < 0.05$. Marker gene selection was performed using nSolver™ 2.0 software. Heatmap depicts mean Nanostring mRNA counts for each marker gene for each cell line normalized to the geometric mean of 78 reference genes. Legend indicates high (red) versus low (blue) expression.

Figure 2 (1 column width). Ingenuity® Pathway Analysis (IPA®) revealed significant overlap between the XDP signature and gene networks related to (**A**) RNA polymerase II ($p = 1.19 \times 10^{-6}$) and (**B**) NFκB ($p = 1.36 \times 10^{-12}$). Interaction modules represent proteins within these cascades with known regulatory relationships to each other. Proteins encoded by XDP marker genes are shown in green (downregulated; XDP vs. control) or red (upregulated; XDP vs. control).

Figure 3 (1 column width). Dose-response curves demonstrating the effects of TNFα on NFκB-luciferase reporter activity in XDP (solid squares; n = 6) vs. control (open squares; n = 6) fibroblasts. The secreted GLuc reporter was assayed in media from replicate fibroblast cultures pre- and post-stimulation (4 h) with the indicated concentration of TNFα. Reporter activity induced by TNFα was calculated for each sample relative to its own baseline and expressed as the fold change relative to the average of untreated cells. XDP fibroblasts exhibited increased mean responses to TNFα compared to control cells. Two-way ANOVA of the dose-response curves revealed significant effects for genotype ($p < 0.0001$) and TNFα ($p < 0.0001$). Data shown represent mean fold changes for each concentration of TNFα ± standard errors.

Figure 4 (1 column width). Western blot analysis confirmed expression of NFκB subunit proteins in whole cell lysates from XDP (n = 6) and control (n = 6) fibroblasts. Representative blots from three independent experiments showed comparative expression across all fibroblast lines of the (**A**) p50 subunit, as well as the p105 precursor protein from which it is proteolytically derived; and (**C**) p65 subunit. Hsp70 was used as a loading control. (**B, D**) Densitometry analysis of western blot data revealed that normalized ratios of p50 and p65 to Hsp70 varied across fibroblast lines, but no significant genotypic differences were detected.

Figure 5 (1 column width). Temporal induction of activated p50 and p65 subunits in response to TNFα in XDP (solid squares; n = 6) vs. control (open squares; n = 6) fibroblasts was assayed using a DNA-binding ELISA for each protein. Data shown in (**A**) and (**B**) represent mean O.D. values normalized to protein input from three independent experiments ± standard errors. (**A**) The timecourse for p50 activation appeared similar in XDP vs. control fibroblasts, but basal and peak levels of DNA-bound p50 were lower in patient cells. Two-way ANOVA of p50 activation profiles revealed significant effects for genotype ($p < 0.001$) and TNFα ($p < 0.001$). (**B**) Activation of the p65 subunit appeared equivalent in XDP vs. control fibroblasts.

Figure 6 (1 column width). Expression of the top three XDP signature genes, *TNFAIP6*, *IL8*, and *CXCL2*, was assayed via qPCR in XDP (solid bars; n = 6) vs. control (open bars; n = 6) fibroblasts following stimulation with 1 ng/mL TNFα for 60 and 90 min. Expression of each gene was normalized to the expression of reference gene, *UBC*. Data shown represent mean fold changes for each target relative to baseline. Mean fold changes for the three genes were compared in XDP vs. control fibroblasts using two-way ANOVA and Sidak's correction for

multiple comparisons, indicating significant differences in induction of *TNFAIP6* and *IL8* at 90 min. ** $p < 0.01$; *** $p < 0.001$. n.s., not significant.

Figure 7 (1 column width). Analysis of NFκB-luciferase reporter expression (**A**) and subunit activation (**B, C**) in XDP vs. control NSC clones. (**A**) Dose-response curves plotting the effects of TNFα on NFκB-luciferase reporter activity in XDP (solid squares; n = 7) and control (open squares; n = 6) NSCs showed a similar pattern as was observed in the fibroblast lines (Fig. 3), with patient cells exhibiting increased mean responses to TNFα compared to controls. Two-way ANOVA of the dose-response curves revealed significant effects for genotype ($p < 0.0001$) and TNFα ($p < 0.0001$). (**B, C**) DNA-binding ELISA for the activated subunits showed robust induction for both p50 (**B**) and p65 (**C**) in XDP (solid bars; n = 7) and control (open bars; n = 6) NSCs stimulated with 1 ng/mL TNFα for given time points, but levels did not vary by genotype.

Figure 8 (1 column width). Expression of 84 NFκB target genes was assayed via qPCR in XDP (n = 7) and control (n = 6) NSCs at baseline (-TNF) and after stimulation with 1 ng/mL TNFα (+TNF). Expression of each target was normalized to the geometric mean of reference genes, *ACTB*, *GAPDH*, *HPRT1*, and *RPLP0*. Heatmap represents log2-transformed ΔCt values for each target in each NSC clone with and without treatment. Legend indicates high (red) versus low (blue) gene expression. Data represent mean results obtained from two biological replicates of each NSC clone.

Figure 9 (1 column width). Contingency table depicting the distribution of mean fold change values (TNFα-treated relative to baseline) for each of the 84 NFκB target genes in XDP (solid

bars; n = 7) vs. control (open bars; n = 6) NSC clones. In control NSCs, 29 of 84 genes (34.5%) showed no response to TNFα compared to only 3 unresponsive genes in XDP NSCs. Chi-square analysis of the distributions revealed a significant effect of genotype (X^2 = 26.3, df = 3, p < 0.0001), indicating broader activation of NFκB target genes in the patient lines.

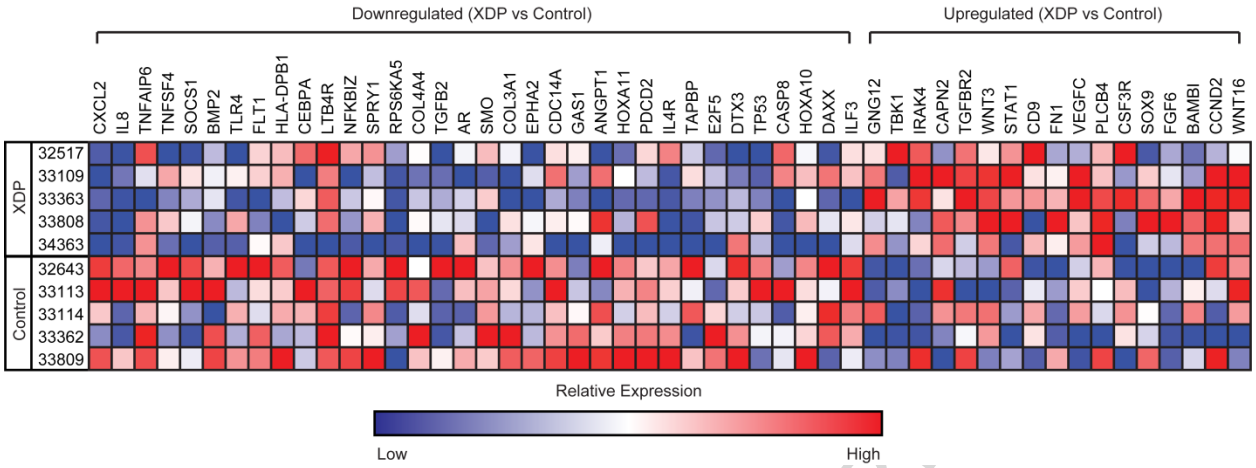

Figure 1

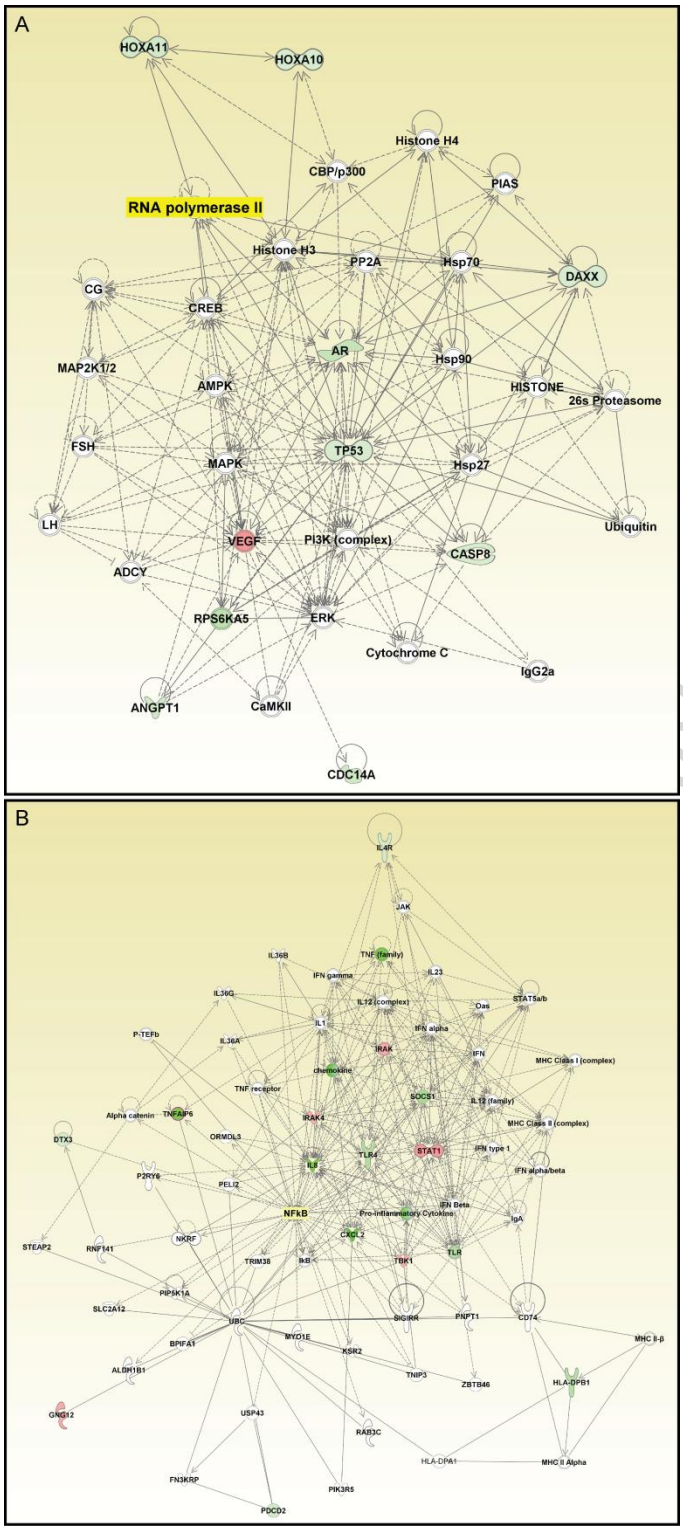

Figure 2

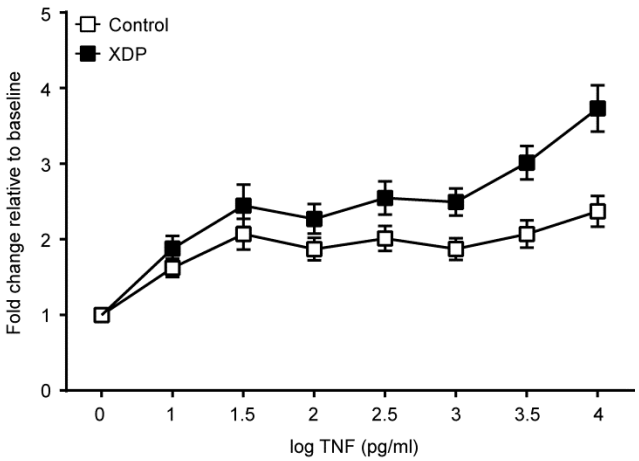

Figure 3

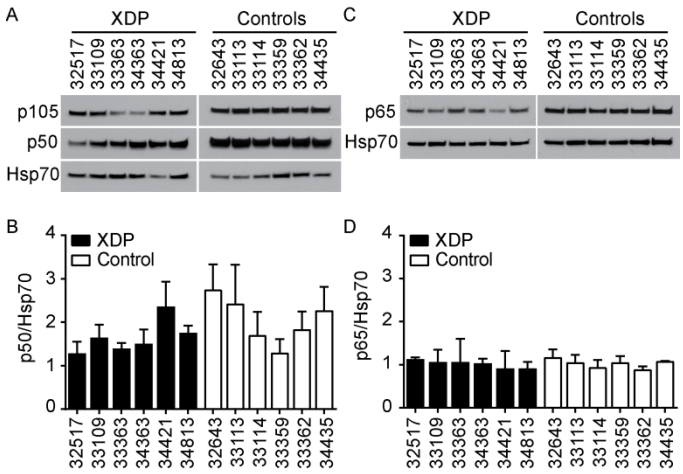

Figure 4

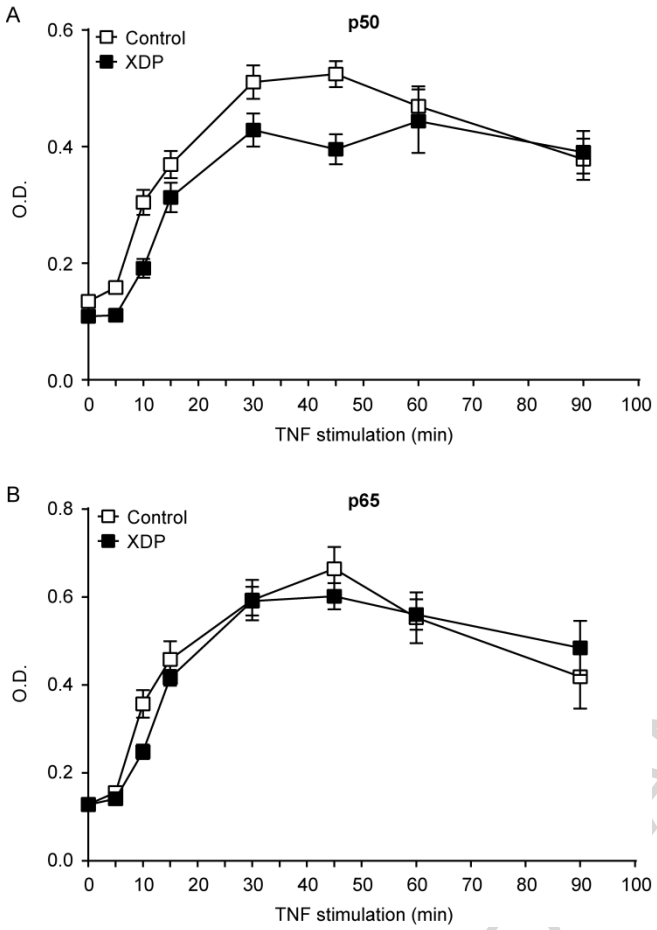

Figure 5

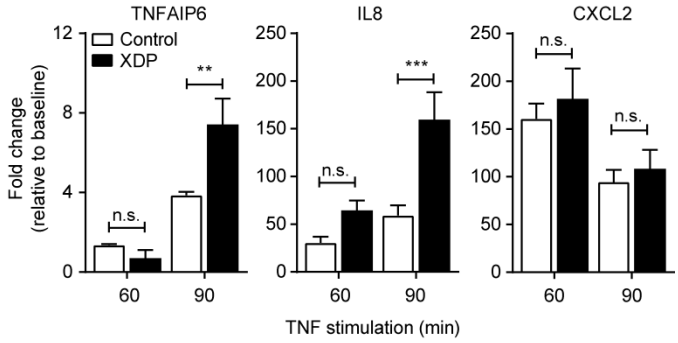

Figure 6

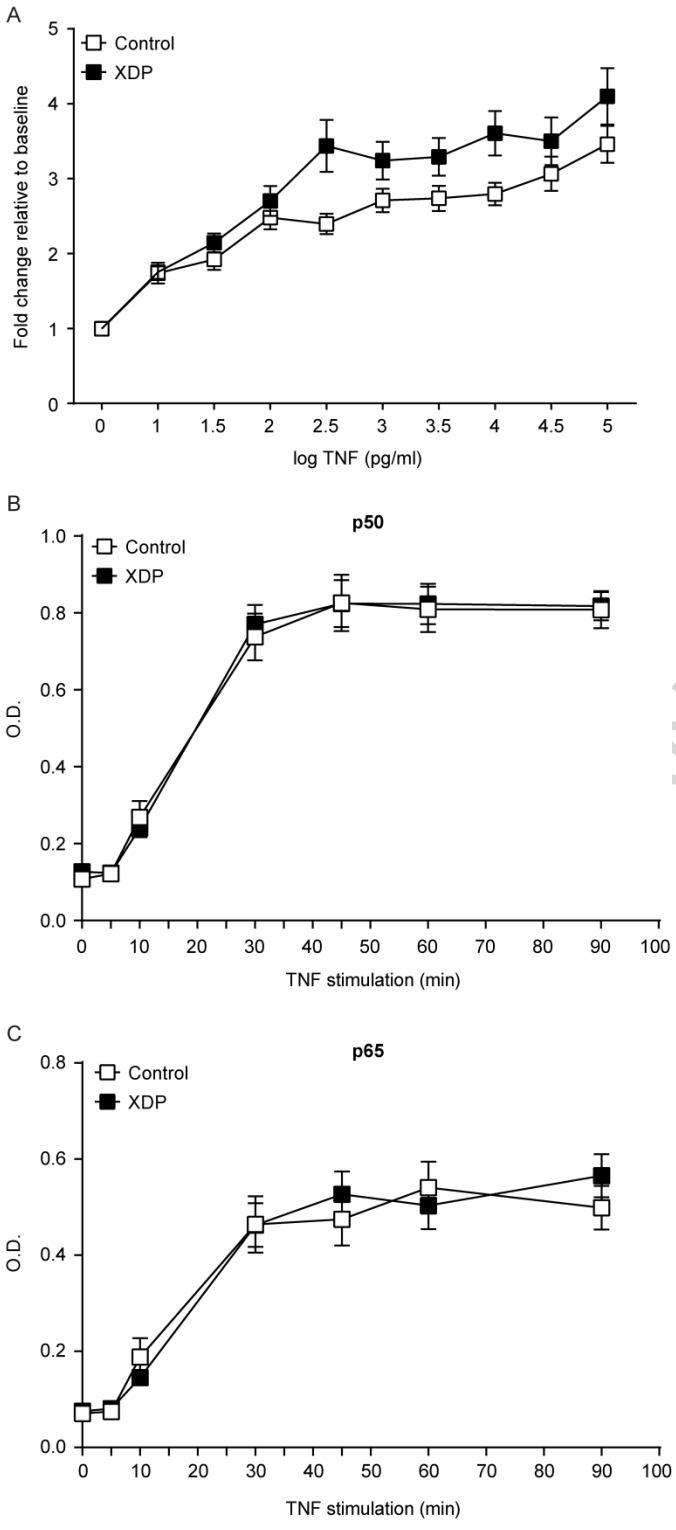

Figure 7

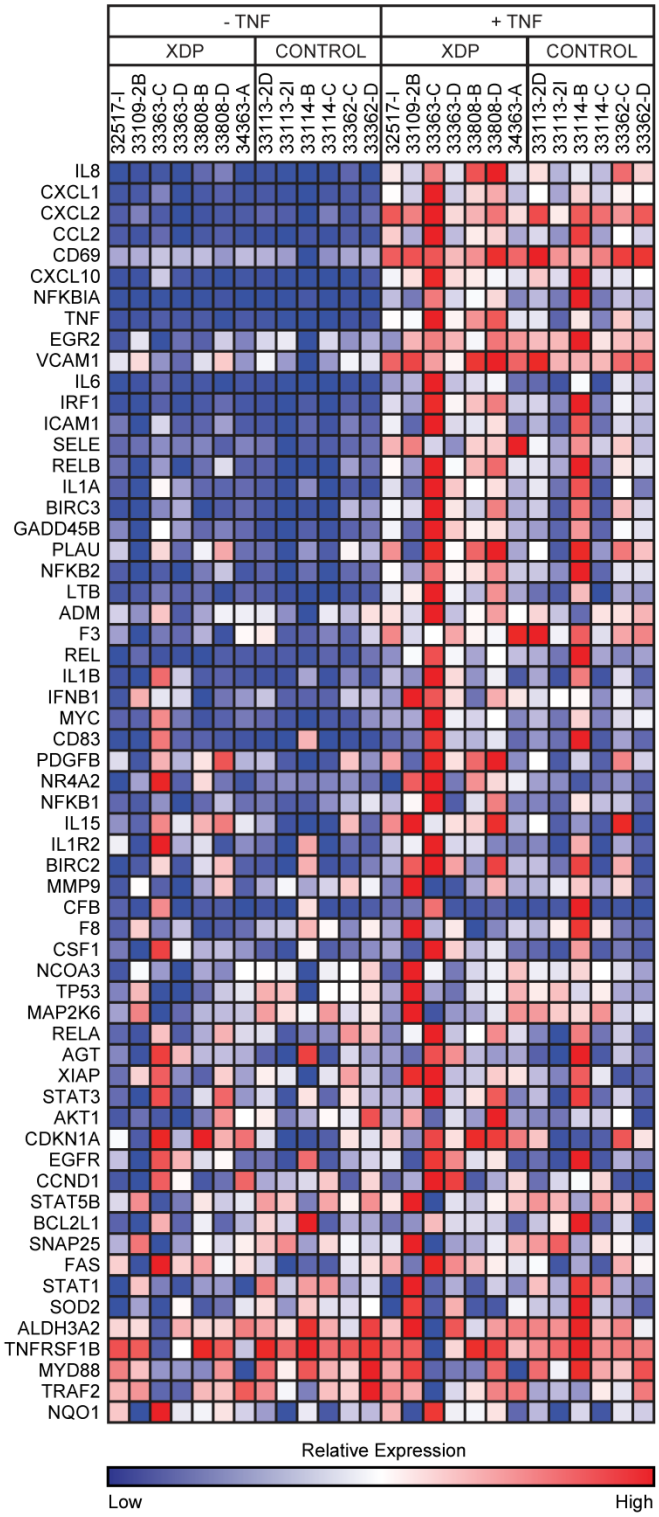

Figure 8

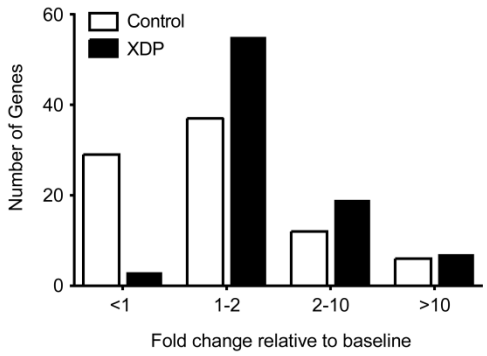

Figure 9